Materials Chemistry and Physics 124 (2010) 646–651

Contents lists available at ScienceDirect

Materials Chemistry and Physics

journal homepage: www.elsevier.com/locate/matchemphys

DTA/TG, IR, EPR and XPS studies of some praseodymium(III) tungstates

S.M. Kaczmarek[a,*], E. Tomaszewicz[b], D. Moszyński[c], A. Jasik[a], G. Leniec[a]

[a] Institute of Physics, Department of Mechanical Engineering and Mechatronics, West Pomeranian University of Technology in Szczecin, Al. Piastów 17, 70-310 Szczecin, Poland
[b] Department of Inorganic and Analytical Chemistry, West Pomeranian University of Technology, Al. Piastów 42, 71-065 Szczecin, Poland
[c] Institute of Chemical and Environment Engineering, West Pomeranian University of Technology, Ul. Pułaskiego 10, 70-322 Szczecin, Poland

ARTICLE INFO

Article history:
Received 15 December 2009
Received in revised form 25 April 2010
Accepted 12 July 2010

Keywords:
Inorganic compounds
Differential thermal analysis (DTA)
Electron paramagnetic resonance
X-ray photo-emission spectroscopy (XPS)

ABSTRACT

The praseodymium(III) tungstates ($Pr_2W_2O_9$ and Pr_2WO_6) have been prepared as polycrystalline powders by thermal treatments of Pr_6O_{11}/WO_3 mixtures in air. It was found the existence of only two polymorphic modification of $Pr_2W_2O_9$. The low-temperature polymorph of $Pr_2W_2O_9$ undergoes reversible polymorphic transition at 1390 K. $Pr_2W_2O_9$ melts incongruently at 1462 K. Low-temperature modification of Pr_2WO_6 is thermally stable up to 1773 K. EPR spectra had shown weak only interactions between tungstate W^{5+} ions that were confirmed also by XPS measurements. Hyperfine structure of W^{4+} ions was also recognized. The spectra characteristics for Pr^{4+} ions were not observed both in EPR and XPS experiments.

1. Introduction

The trivalent metal molybdates and tungstates include a number of materials with interesting fluorescent, laser, piezoelectric, ferroelectric and ferroelastic properties. The special group of these compounds is family of rare-earth metal molybdates and tungstates. These compounds adopt a large number of different structures and many of them display negative thermal expansion.

In the Pr_2O_3–WO_3 system, the following praseodymium(III) tungstates are known: $Pr_2(WO_4)_3$ (Pr_2O_3:WO_3 – 1:3); $Pr_2W_2O_9$ (1:2); $Pr_8W_5O_{27}$ (4:5); Pr_2WO_6 (1:1); $Pr_6W_2O_{15}$ (3:2) and probably Pr_6WO_{12} (3:1) [1–7]. Praseodymium(III) tungstate ($Pr_2W_2O_9$), belonging to the family of isostructural compounds $RE_2W_2O_9$ (*RE* = Ce-Gd), shows polymorphism [6,7]. The low-temperature polymorphic modification (II-$Pr_2W_2O_9$) crystallizes in the monoclinic system, in the $P2_1/c$ space group and with the following lattice parameters: $a = 0.770$ nm; $b = 0.984$ nm; $c = 0.927$ nm; $\beta = 106.5^\circ$; $Z = 4$ [6,7]. Its structure consists of endless, zigzag chains $[(W_2O_9)^{6-}]_\infty$ created by connecting the WO_6 octahedra by one common edge [6] (Fig. 1). The praseodymium(III) ions are present in two different oxygen coordination environments, i.e. PrO_8 (ditrigonal prism) and PrO_9 (tritrigonal prism) [6]. The high-temperature modification (I-$Pr_2W_2O_9$) crystallizes in the cubic system with the lattice constant $a = 0.7105$ nm and $Z = 2$ [6]. The polymorphic transition of II-$Pr_2W_2O_9$ to I-$Pr_2W_2O_9$ occurs at 1393 K [7]. Reznik and Ivanova [7] suggested that $Pr_2W_2O_9$ has got third polymorphic modification existing up to 593 K [7]. The other praseodymium(III) tungstate (Pr_2WO_6) possesses two polymorphs [6,7]. The low-temperature polymorphic form (II-Pr_2WO_6) crystallizes in the monoclinic system (the space group $C2/c$) and has the following parameters of the unit cell: $a = 1.6691$ nm; $b = 1.4436$ nm; $c = 0.5546$ nm; $\beta = 107.54^\circ$ [6,8]. Deformed, isolated trihedral bipyramides, WO_5, and three deformed, non-equivalent PrO_8 cubes are observed in the structure of this modification [6] (Fig. 2). The high-temperature form (V-Pr_2WO_6) crystallizes in the orthorhombic system with the lattice constants: $a = 0.5394$ nm; $b = 0.9274$ nm; $c = 1.0241$ nm [6]. The polymorphic transition of II-form to V-modification occurs at 1823 K [7]. Pr_2WO_6 melts incongruently at 1948 K [6].

In this paper, we completed the previous experimental data related with thermal properties of $Pr_2W_2O_9$. Particularly, we have studied and analyzed EPR and XPS spectra of the II-$Pr_2W_2O_9$ and II-Pr_2WO_6 phases.

2. Experimental

2.1. Sample preparation

Polycrystalline samples of $Pr_2W_2O_9$ and Pr_2WO_6 were prepared by the solid-state reaction according to the following equations:

$$Pr_6O_{11(s)} + 6\,WO_{3(s)} = 3\,Pr_2W_2O_{9(s)} + O_{2(g)} \quad (1)$$

$$Pr_6O_{11(s)} + 3\,WO_{3(s)} = 3\,Pr_2WO_{6(s)} + O_{2(g)} \quad (2)$$

The reagents (Pr_6O_{11}, 99.9% Aldrich; WO_3, 99.9% Fluka) were weighed in appropriate ratios and ground in an agate mortar. The obtained mixtures were heated in the air in the following cycles: 1073 K (12 h); 1173 K (12 h); 1273 K (12 h) and 1323 K (12 h). For better reactivity, the Pr_6O_{11}/WO_3 mixtures were ground in an agate mortar after each 12-h period of annealing. The XRD measurements of the samples obtained after

* Corresponding author.
E-mail addresses: skaczmarek@zut.edu.pl, skaczmarek@ps.pl (S.M. Kaczmarek).

0254-0584/$ – see front matter © 2010 Elsevier B.V. All rights reserved.
doi:10.1016/j.matchemphys.2010.07.028

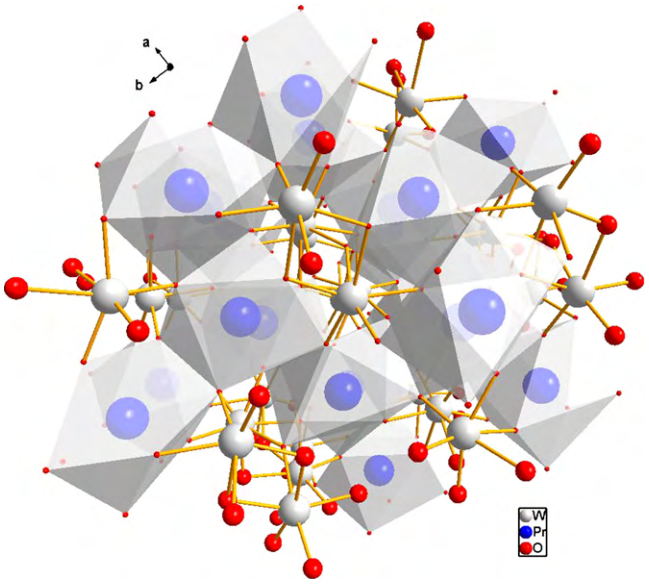

Fig. 1. Crystal structure of II-$Pr_2W_2O_9$ [6].

the last heating cycle of $Pr_6O_{11}/6WO_3$ and $Pr_6O_{11}/3WO_3$ mixtures have shown that they contain only II-$Pr_2W_2O_9$ and II-Pr_2WO_6, respectively.

2.2. Measurements

Powder X-ray diffraction patterns were collected within the range from 10° to 52° 2θ with a step 0.02° 2θ and counting time 1 s per step on a DRON-3 diffractometer with Cu Kα radiation (λ = 0.15418 nm).

DTA-TG studies were performed on a TA Instruments thermoanalyzer (Model SDT 2960) at the heating or cooling rate of 10 K min^{-1} to the maximum temperature of 1773 K and in the air and an inert atmosphere (nitrogen, 99.996%) with the gas flow 110 mL h^{-1}.

Infrared spectral data were collected on a Specord M80 spectrophotometer in the range of 300–1200 cm^{-1} using KBr pellets.

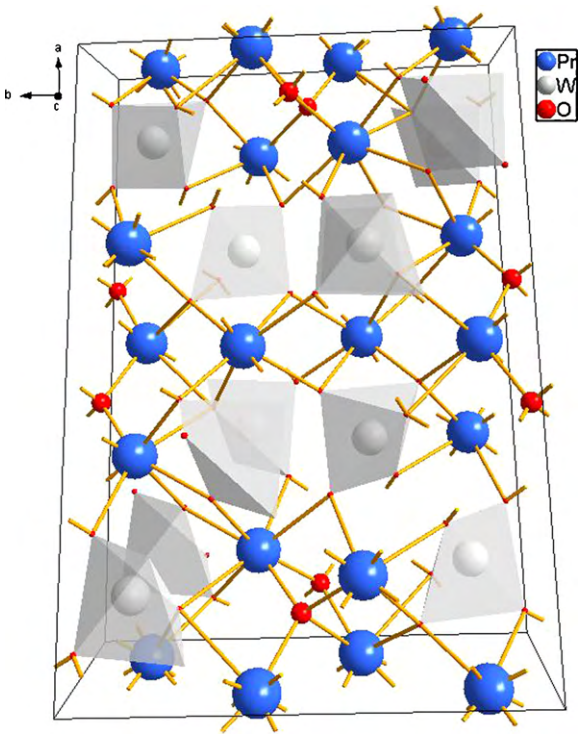

Fig. 2. Crystal structure of II-Pr_2WO_6 [8].

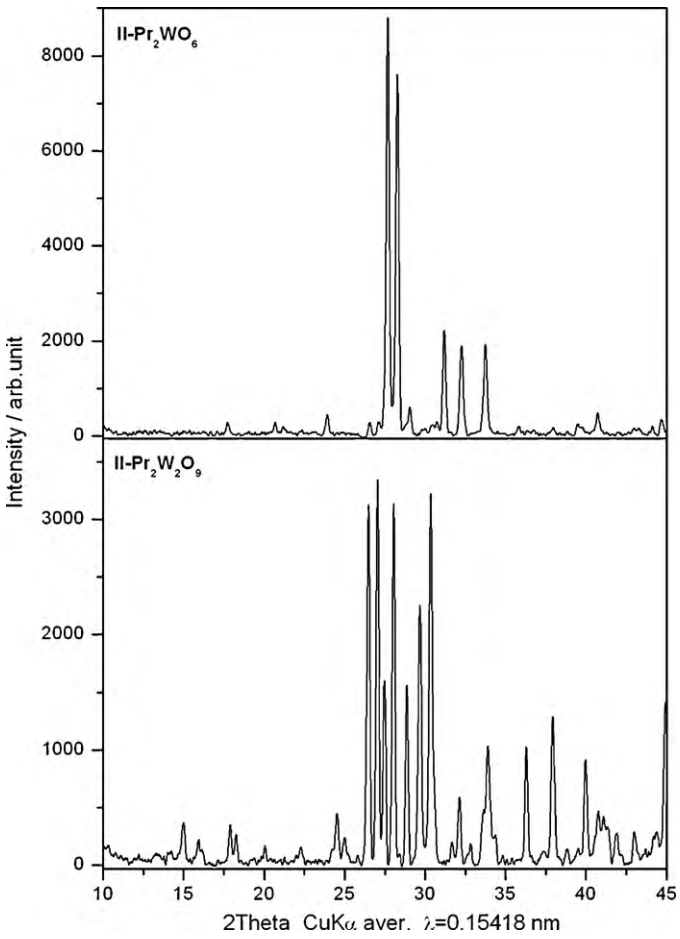

Fig. 3. XRD patterns of II-Pr_2WO_6 and II-$Pr_2W_2O_9$.

EPR spectra were recorded on a conventional X-band Bruker ELEXSYS E 500 CW-spectrometer operating at 9.5 GHz with 100 kHz magnetic field modulation. The investigated samples were in fine powder form. The first derivative of the powder absorption spectra has been recorded as a function of the applied magnetic field. Temperature dependence of the EPR spectra of the powder sample in the 90–300 K temperature range was recorded using an Oxford Instruments ESP nitrogen-flow cryostat.

XPS studies were carried out with use of the Prevac electron spectrometer, equipped with SES 2002 (VG Scienta) electron energy analyzer working in Constant Energy Aperture mode. Samples were excited with Mg Kα radiation. The spectra were acquired with pass energy of 50 eV. Calibration of the energy scale was done prior to analysis basing on Ag 3d transition. A shift of XPS lines due to the charging of the surface was observed and it was corrected numerically during analysis of the spectra. It was assumed that carbon C 1 s line should be placed at 284.6 eV (adventitious carbon) and the positions of other XPS lines were shifted accordingly.

3. Results and discussion

3.1. XRD and DTA–TG studies

Fig. 3 shows XRD patterns of the II-$Pr_2W_2O_9$ and II-Pr_2WO_6 phases. The position and relative intensity of each diffraction line recorded on X-ray powder diffraction patterns of low polymorphic modification of $Pr_2W_2O_9$ as well as II-Pr_2WO_6 are in very good accordance with the suitable data for these phases reported by the International Centre for Diffraction Data [9].

Figs. 4 and 5 show DTA and TG curves of $Pr_2W_2O_9$ recorded during heating of this compound in two different atmospheres. The first endothermic effect with its onset at 1389 K (nitrogen atmosphere, Fig. 5) or at 1390 K (air, Fig. 4) not associated with mass change of the samples, corresponds to a polymorphic transition of II-$Pr_2W_2O_9$ to I-$Pr_2W_2O_9$. These values of transition temperature

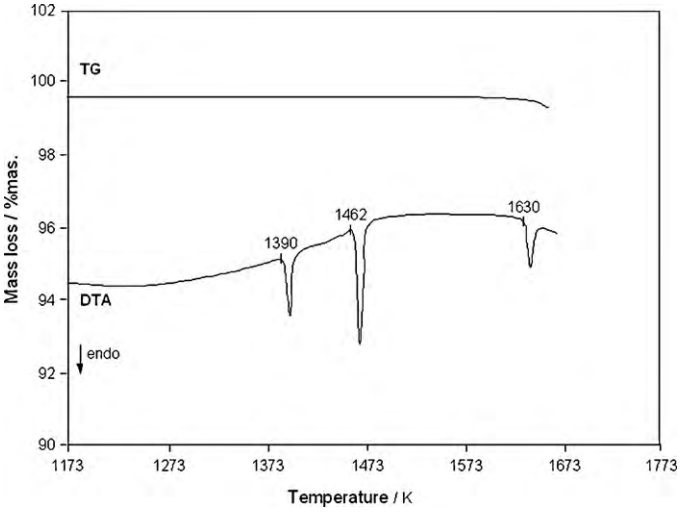

Fig. 4. DTA–TG curves of $Pr_2W_2O_9$ (air atmosphere).

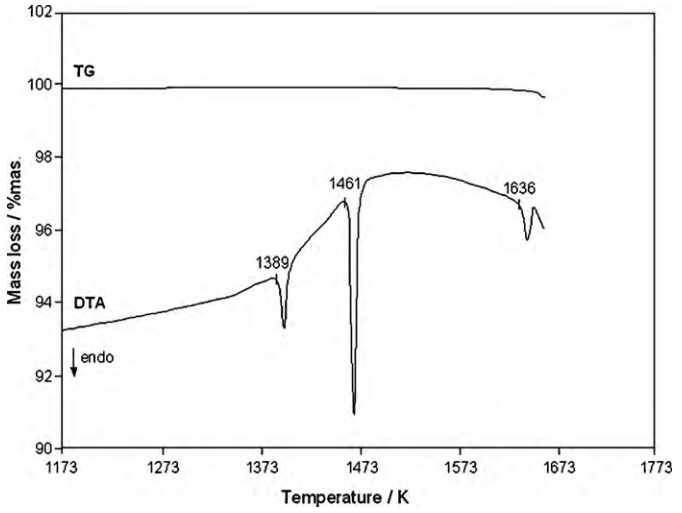

Fig. 5. DTA–TG curves of $Pr_2W_2O_9$ (nitrogen atmosphere).

are close to the value obtained earlier [7]. This transformation is associated with a change of crystallographic structure of $Pr_2W_2O_9$ (monoclinic II-$Pr_2W_2O_9$ → cubic I-$Pr_2W_2O_9$). The second endothermic effect recorded on the DTA curve of $Pr_2W_2O_9$ at 1461 K (N_2 atmosphere, Fig. 5) or at 1462 K (air, Fig. 4) is connected with incongruent melting of $Pr_2W_2O_9$. No mass loss associated with this endothermic effect was observed on the TG curves recorded during DTA–TG studies made in different atmospheres (Figs. 4 and 5). The process of incongruent melting can be described by the following equation:

$$Pr_2W_2O_{9(s)} \leftrightarrows Pr_8W_5O_{27(s)} + \text{liquid} \quad (3)$$

Melting manner of $Pr_2W_2O_9$ confirms the third endothermic effect appearing on the DTA curve of this compound at 1630 K (air, Fig. 4) or at 1636 K (nitrogen atmosphere, Fig. 5). This effect is associated with incongruent melting of $Pr_8W_5O_{27}$ [6]. The mass loss connected with the evaporation of liquid and corresponding only to the third endothermic effect was observed on the both TG curves (Figs. 4 and 5).

Fig. 6 shows DTA curves of $Pr_2W_2O_9$ recorded in air as well as in inert atmosphere during heating this phase up to 1433 K and DTA curves recorded during controlled cooling down to 1073 K. The exothermic effect with its onset at 1384 K (inert atmosphere,

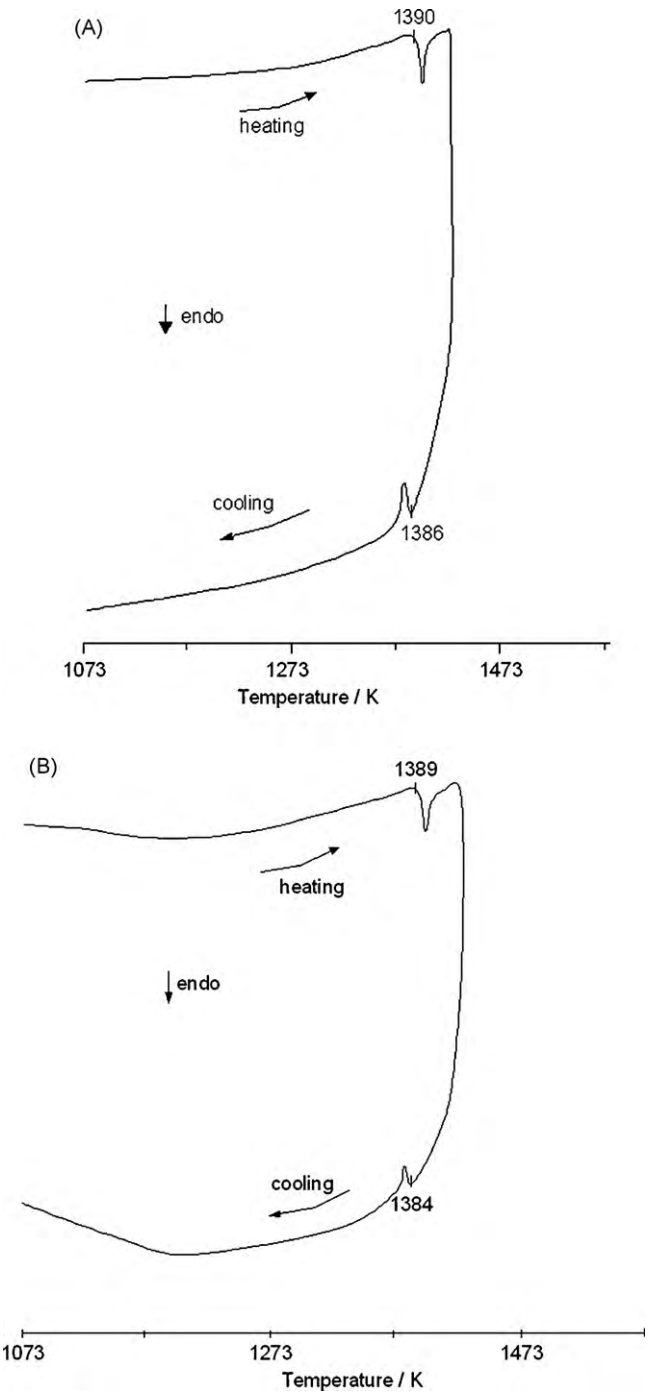

Fig. 6. DTA curves of II-$Pr_2W_2O_9$ recorded during heating up to 1433 K and next cooling to 1073 K ((A) air; (B) nitrogen atmosphere).

Fig. 6A) or at 1386 K (air, Fig. 6B) is connected with crystallization of a low-temperature form of $Pr_2W_2O_9$. It means that the polymorphic transition of II-$Pr_2W_2O_9$ to I-$Pr_2W_2O_9$ is reversible. On the DTA curve of Pr_2WO_6 (not presented here) any effects were recorded up to 1773 K.

3.2. IR spectra

Fig. 7 shows IR spectra of II-$Pr_2W_2O_9$ (spectrum A) and II-Pr_2WO_6 (spectrum B). IR spectrum of II-$Pr_2W_2O_9$ shows a big similarity to the infrared spectrum of this compound previously recorded by other authors [10]. Based on the literature information

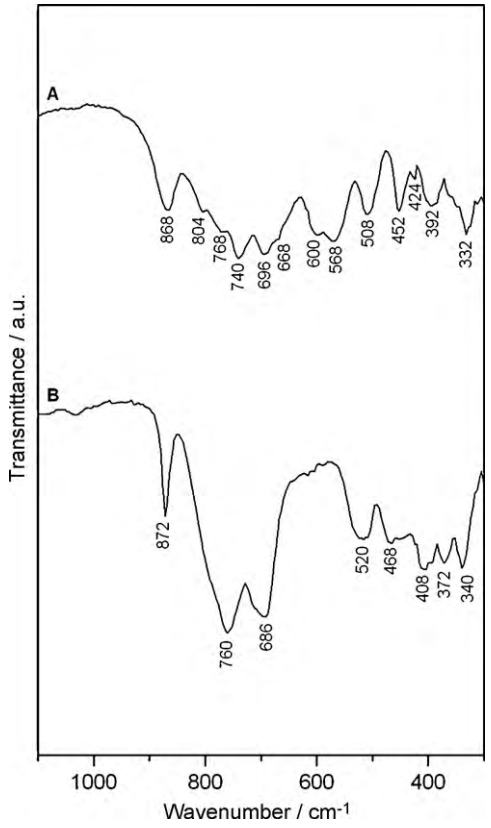

Fig. 7. IR spectra of II-$Pr_2W_2O_9$ (A) and II-Pr_2WO_6 (B).

[10,11] the absorption band recorded for II-$Pr_2W_2O_9$ with the maximum at 868 cm^{-1} is due to the stretching modes of W–O bonds in joint WO_6 octahedra forming the structure elements $[(W_2O_9)^{6-}]_\infty$. The several absorption bands in the 804–508 cm^{-1} region can be assigned to the asymmetric stretching vibration of W–O bonds in joint WO_6 octahedra and also to the oxygen double bridge bonds WOOW [10]. The absorption bands below 500 cm^{-1} can be assigned to the symmetric and also asymmetric deformation modes of W–O bonds as well as to the deformation modes of the oxygen bridges WOOW [9]. The II-Pr_2WO_6 spectrum has not yet been presented in a literature. This spectrum shows a big similarity to the IR spectra of other isostructural rare-earth metal tungstates RE_2WO_6 [11]. The absorption band with its maximum at 872 cm^{-1} can be due to the stretching modes of W–O bonds in isolated trihedral bipyramides WO_5 [11]. The absorption bands at 760 and 686 cm^{-1} can be assigned to the asymmetric stretching modes of W–O bonds in WO_5. Several absorption bands with their maxima recorded below 600 cm^{-1} can be due to the deformation modes of W–O bonds in WO_5 [11].

3.3. EPR spectra

A group of II-$Pr_2W_2O_9$ and II-Pr_2WO_6 powders investigated by using the EPR technique revealed existence of the X-band weak resonance signal in whole temperature range up to 300 K. The EPR results are shown in Fig. 8. The shape of the EPR lines is the same for both powders and consists mainly of one sharp line with $g = 2.07$ (Fig. 8a), although the line seem to be a superposition of at least two different lines. The position of the first line, centered at $g = 2.07$ changes with a temperature over 60 K suggesting the presence of some internal magnetic field in the sample. About 17 K there clearly arise second type line in the EPR spectrum, centered at about $g = 2.75$ (Fig. 8b). It leads to a complex behaviour of a temperature dependence of a total integrated intensity. EPR integrated intensity, χ_{EPR}, is calculated as an area under the absorption EPR spectrum and is usually proportional to the magnetic susceptibility of the investigated spin system. From our investigations it results that the Curie–Weiss law applied to the integrated intensity is satisfied only in the temperature range below 17 K. The least-square fitting of the experimental points to the Curie–Weiss law produced $T_{CW} = 4$ K for II-Pr_2WO_6 sample and $T_{CW} = 0.3$ K for II-$Pr_2W_2O_9$ sample indicating on a weak ferromagnetic interaction between paramagnetic ions. It was confirmed also by a shape of $\chi_{EPR} \times T$ dependence on a temperature. In general, this product is proportional to the square root of an effective magnetic moment. For the II-Pr_2WO_6 and II-$Pr_2W_2O_9$ the effective magnetic moment decreases with temperature decrease in high-temperature range ($T > 60$ K), but increases in low-temperature range below 17 K for II-Pr_2WO_6 and stay close to zero for II-$Pr_2W_2O_9$. Thus, the dominating antiferromagnetic interaction at high-temperature changes to a weak ferromagnetic interaction at low-temperature. Over 30 K one can observe also 4-fold signal of hyperfine interaction type that disappears at about 50 K (Figs. 8c and 9). We suggest that the observed resonance line isn't

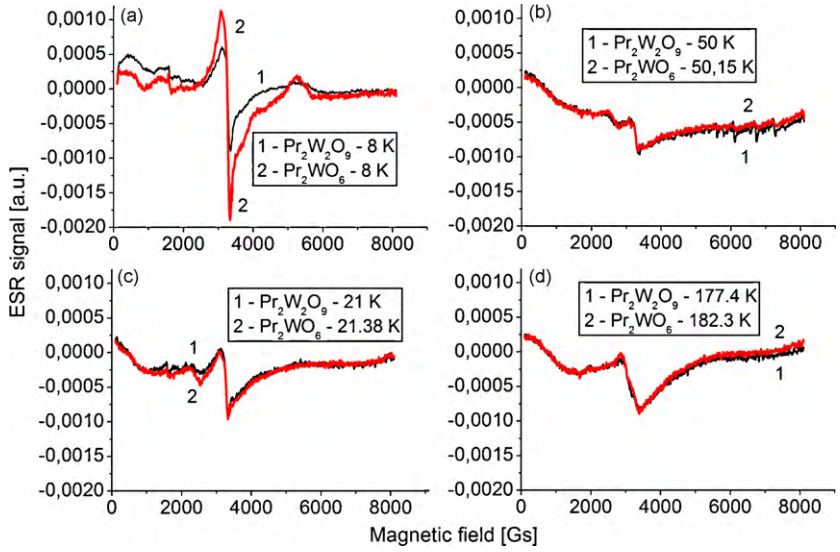

Fig. 8. Temperature dependence of EPR spectra for II-$Pr_2W_2O_9$ and II-Pr_2WO_6 samples at ~8 K (a), ~21 K (b), ~50 K (c) and ~180 K (d).

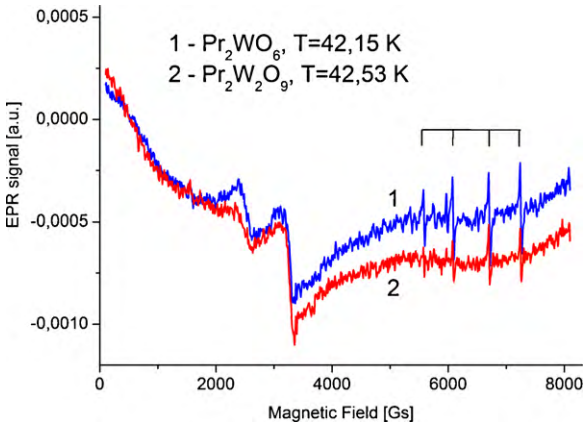

Fig. 9. EPR spectra of II-Pr_2WO_6 (1) and II-$Pr_2W_2O_9$ (2) samples at temperatures 42.15 and 42.53 K, respectively.

attributed to the Pr^{4+} ions but to tungstate W^{5+} and W^{4+} ones [12].

According to the crystal structure of typical double tungstates and molybdates, they nominally could consist of two kinds of paramagnetic centres: rare-earth RE^{3+} ions with C_2 or lower point symmetry located at distorted dodecahedra and/or reduced transition metal Me^{5+} ions located at octahedral sites. The tungsten or molybdate center is expected to undergo two subsequent one-electron reductions from Me^{6+} to Me^{4+}. The intermediate Me^{5+} is paramagnetic and shows a typical $S = 1/2$ signal with all g values usually below 2.0, which is still observable at temperatures as high as 100 K [13]. In our samples there arise at least two non-equivalent positions of W^{6+} (so also W^{5+}) ions that form chains of octahedral. The complex EPR spectrum we observed, consisting of at least two lines, suggests the presence of at least two types of paramagnetic entities, what clearly agree with a structure of the investigated samples. A change in the EPR line position suggests magnetic interaction between chains built of tungsten octahedra. The 4-fold signal of hyperfine interaction, centered at $g = 1.210$, 1.110, 1.007 and 0.932 seem to be a hyperfine structure of ^{183}W isotope (~14% abundance) with an electron spin $S = 1$ and nuclear $I = 1/2$.

The EPR results for both praseodymium tungstates suggest that transition metal ions are well isolated each other in these types of structures, showing insignificant magnetic interaction.

3.4. XPS studies

II-Pr_2WO_6 and II-$Pr_2W_2O_9$ phases have also been analyzed by XPS method. The XPS Pr 3d lines for both compounds are shown in Fig. 10. The XP spectra are virtually identical for both samples. There are two distinct bands corresponding with the spin-orbit doublet Pr $3d_{5/2}$ and Pr $3d_{3/2}$. The maxima of Pr $3d_{5/2}$ core level peaks were found to be at 933.1 ± 0.1 eV with the energy separation between Pr $3d_{5/2}$ and Pr $3d_{3/2}$ components being equal to 20.5 eV. The positions of the peaks are in good agreement with the literature values characteristic for praseodymium oxidation state Pr^{3+} [14]. At the side of lower binding energies there is a well-defined shoulder ascribed to the shake-off satellite [15,16]. The presence of Pr^{4+} oxidation state should produce the spectral line at 935.5 eV with the separation energy to Pr $3d_{3/2}$ spin-orbit component equal to 17.8 eV [17]. With the lack of these components in the XPS Pr 3d spectrum there are no evidences on the existence of Pr^{4+} oxidation state in the samples. However, considering relatively small sensitivity of XPS method, the presence of small quantities of Pr^{4+} ions, probably mainly at the grain boundaries of both analyzed powdered samples, cannot be excluded.

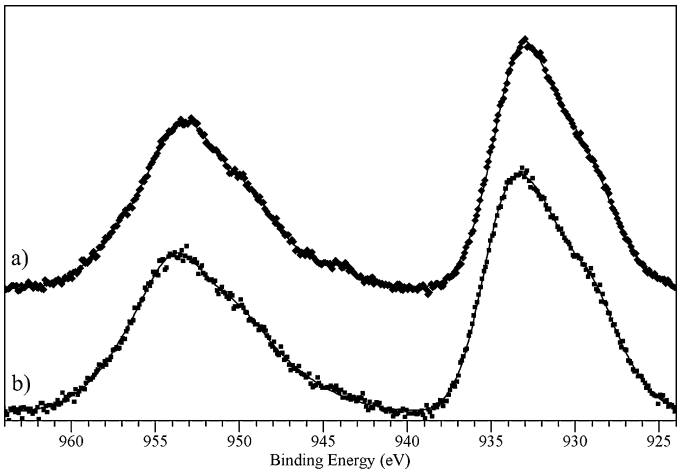

Fig. 10. XPS Pr 3d lines for II-Pr_2WO_6 (a) and II-$Pr_2W_2O_9$ (b) compounds.

In Fig. 11 the XP spectra of W 4f lines for both praseodymium compounds, two gadolinium tungstates, $Gd_2W_2O_9$ and II-Gd_2WO_6, which are isostructural to adequate praseodymium tungstates, as well as for WO_3 are presented. XPS data measured for these samples are shown in Table 1. All of W 4f lines were peak-fitted and their respective components are shown as thin lines in Fig. 11. W 4f line contains two spin-orbit components W $4f_{7/2}$ and W $4f_{5/2}$, respectively. In a case of pure WO_3 the maximum of W $4f_{7/2}$ line was found to be at binding energy 35.7 eV, and is in good agreement with peaks originating from W^{6+} oxidation states in WO_6 octahe-

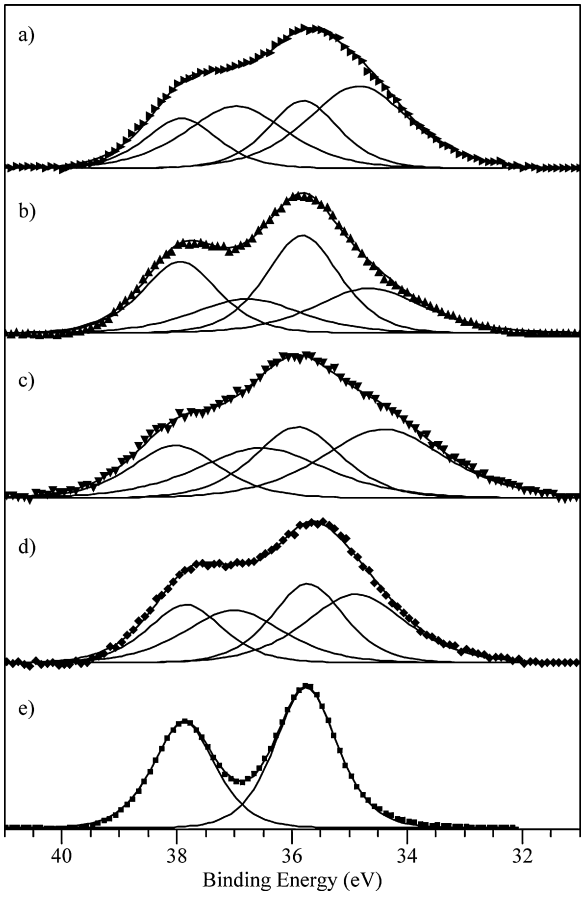

Fig. 11. XPS W 4f lines for II-$Pr_2W_2O_9$ (a), $Gd_2W_2O_9$ (b), II-Pr_2WO_6 (c), II-Gd_2WO_6 (d) and WO_3 (e).

Table 1
XPS data measured for II-Pr_2WO_6, II-$Pr_2W_2O_9$, II-Gd_2WO_6, $Gd_2W_2O_9$ and WO_3.

	II-Pr_2WO_6		II-$Pr_2W_2O_9$		II-Gd_2WO_6		$Gd_2W_2O_9$		WO_3	
	BE (eV)	FWHM (eV)	BE (eV)	FWHM (eV)	BE (eV)	FWHM (eV)	BE (eV)	FWHM (eV)	BE (eV)	FWHM (eV)
W $4f_{7/2}$	35.9	1.8	35.8	1.4	35.7	1.5	35.8	1.5	35.7	1.3
	34.4	2.5	34.8	2.1	34.9	2.1	34.7	2.2		
W $4f_{5/2}$	38.0	1.8	37.9	1.5	37.8	1.5	37.9	1.5	37.8	1.3
	36.5	2.6	36.9	2.1	37.0	2.0	36.8	2.2		

dra [18,19]. The W 4f lines for all materials containing rare-earth ions are composed of two pairs of components. One of them can be definitely ascribed to W^{6+} oxidation states as in WO_3 and their binding energies are 35.8 ± 0.1 eV. However, there is an additional component present in all rare-earth metal tungstates. Its maximum has been found at binding energy 34.7 ± 0.2 eV. This position is in the middle of the binding energies characteristic for W^{6+} (about 35.5 eV) and W^{4+} (about 32.5 eV) known from the literature [20]. The presence of an additional component in W 4f spectra of both investigated gadolinium tungstates (gadolinium can exist only in +3 oxidation state) puts in doubt the existence of W^{5+} oxidation state. It seems that the presence of low binding energy component in W 4f spectra of compounds under study is a reflection of prominent deformation of their crystal structure only at the surface of grains. The presence of vacancies in the anion sublattice due to an oxygen deficiency leads to the change of chemical state of tungsten ions and the presence of additional peak in XPS W 4f line. Very similar change of the XPS W 4f line shape was previously observed for nonstoichiometric WO_{3-x} oxides [18,21].

4. Conclusions

Two praseodymium(III) tungstates II-$Pr_2W_2O_9$ and II-Pr_2WO_6 were synthesized by the high-temperature solid-state reaction between Pr_6O_{11} and WO_3. On the basis of DTA studies it was confirmed the existence of only two $Pr_2W_2O_9$ polymorphic modifications. Regardless of the type used gas for DTA–TG experiments, low-temperature polymorph of $Pr_2W_2O_9$ undergoes reversible polymorphic transition practically at the same temperature, i.e. at about 1390 K. The I-$Pr_2W_2O_9$ phase melts incongruently at about 1462 K both in the air and inert gas. Low-temperature form of Pr_2WO_6 is thermally stable up to 1773 K. EPR results have shown a weak magnetic interaction between tungstate ions in both powder samples indicating on a good enough isolation between them in the structure. The resonance signal is coming mainly from W^{5+} (only hyperfine structure of the EPR spectra indicates on the presence of the W^{4+} ions) arising in the compounds due to two subsequent one-electron reductions from W^{6+} to W^{4+}. XPS measurements confirm the conclusion. There have not been observed Pr^{4+} ions both in EPR and XPS experiments.

References

[1] M. Yoshimura, H. Morikawa, M. Miyake, Mater. Res. Bull. 10 (1975) 1221.
[2] K. Nassau, H.J. Levinstein, J.M. Loiacini, J. Phys. Chem. Solids 26 (1965) 1805.
[3] L.N. Brixner, A.W. Sleight, Mater. Res. Bull. 8 (1973) 1269.
[4] I.N. Belaev, L.A. Voropanova, Zh. Neorg. Khim. 19 (1974) 3388 (in Russian).
[5] V.K. Trunov, O.V. Kubin, Zh. Neorg. Khim. 22 (1977) 1184 (in Russian).
[6] A.A. Evdokimov, V.A. Ephremov, V.K. Trunov, I.A. Klejnman, B.F. Dzhurinskij, Soedineniya Redkozemelykh Elementov. Molibdaty, Volframaty, in: I.V. Tananaev, V.K. Trunov (Eds.), Compounds of Rare Earth Elements. Molybdates, Tungstates, Nauka, Moscow, 1991 (in Russian).
[7] E.M. Reznik, M.M. Ivanova, Zh. Neorg. Khim. 21 (1976) 522 (in Russian).
[8] P.S. Berdonosov, D.O. Charkin, K.S. Knight, K.E. Johnston, R.J. Goff, V.A. Dolgikh, P. Lightfoot, J. Solid State Chem. 179 (2006) 3437.
[9] International Centre for Diffraction Data: The Cards No.: 21-0739, pp. 31–1153.
[10] V.V. Fomiczev, O.I. Kondratov, V.A. Gagarina, K.I. Petrov, Zh. Neorgan. Khim. 23 (1978) 87 (in Russian).
[11] V.I. Tsaryuk, V.F. Zolin, Spectrochim. Acta A57 (2001) 355.
[12] Y. Hinatsu, N. Edelstein, J. Solid State Chem. 112 (1994) 53.
[13] A.D. Prokhorov, M.T. Borowiec, V.P. Dyakonov, V.I. Kamenev, A.A. Prokhorov, P. Aleshkevych, T. Zayarnyuk, H. Szymczak, Physica B 403 (2008) 3174.
[14] A. Mekki, K.A. Ziq, D. Holland, C.F. McConville, J. Magn. Magn. Mater. 260 (2003) 60.
[15] D. Schmeisser, Mater. Sci. Semicond. Process. 6 (2003) 59.
[16] H. Ogasawara, A. Kotani, R. Potze, G.A. Sawatzky, B.T. Thole, Phys. Rev. B 44 (1991) 5465.
[17] Y. Uwamino, I. Ishizuka, H. Yamatera, J. Electron. Spectrosc. Relat. Phenom. 34 (1984) 67.
[18] O.Y. Khyzhun, J. Alloys Compd. 305 (2000) 1.
[19] O.Y. Khyzhun, Y.M. Solonin, V.D. Dobrovolsky, J. Alloys Compd. 320 (2001) 1.
[20] J.F. Moulder, W.E. Stickle, P.E. Sobol, K.E. Bomben, in: J. Chastian (Ed.), Handbook of X-ray Photoelectron Spectroscopy, Perkin-Elmer, Eden Prairie, Minnesota, 1992.
[21] F. Bussolotti, L. Lozzi, M. Passacantando, S. La Rosa, S. Santucci, L. Ottaviano, Surface Sci. 538 (2003) 113.